Soft Matter

Accepted Manuscript

ROYAL SOCIETY OF CHEMISTRY

www.rsc.org/softmatter

Journal Name

ARTICLE TYPE

Cite this: DOI: 10.1039/xxxxxxxxxx

Hydrodynamic oscillations and variable swimming speed in squirmers close to repulsive walls

Juho S. Lintuvuori,[a] Aidan T. Brown,[b] Kevin Stratford [c] and Davide Marenduzzo [b]

Received Date
Accepted Date

DOI: 10.1039/xxxxxxxxxx

www.rsc.org/journalname

We present a lattice Boltzmann study of the hydrodynamics of a fully resolved squirmer, confined in a slab of fluid between two no-slip walls. We show that the coupling between hydrodynamics and short-range repulsive interactions between the swimmer and the surface can lead to hydrodynamic trapping of both pushers and pullers at the wall, and to hydrodynamic oscillations in the case of a pusher. We further show that a pusher moves significantly faster when close to a surface than in the bulk, whereas a puller undergoes a transition between fast motion and a dynamical standstill according to the range of the repulsive interaction. Our results critically require near-field hydrodynamics and demonstrate that far-field hydrodynamics is insufficient to give even a qualitatively correct account of swimmer behaviour near walls. Finally our simulations suggest that it should be possible to control the density and speed of squirmers at a surface by tuning the range of steric and electrostatic swimmer-wall interactions.

1 Introduction

Motile organisms such as bacteria and sperm cells have a natural tendency to be attracted towards surfaces, and to swim near them[1]. This phenomenon may be relevant for the initial stage of the formation of biofilms, the microbial aggregates which often form on surfaces. However, experiments have shown that this tendency is not unique to living swimmers, and is also exhibited by phoretic, synthetic active particles[2–4]: in that context, it has been exploited for example, to attract microswimmers inside a colloidal crystal, where they orbit around the colloids[4]. The interaction between self-propelled particles and walls also provides a microscopic basis for the rectification of bacterial motion by asymmetric geometries (*e.g.* funnels)[5].

Previous work has proposed two possible mechanisms for surface accumulation of self-motile particles. A first view is that accumulation occurs through far-field hydrodynamic interactions[6]. Another possibility is that motility itself, in the absence of solvent-mediated interactions, leads to accumulation[7,8]: this mechanism requires a small enough channel, where the gap size is of the order of the typical distance travelled ballistically by the active particles, before rotational diffusion or tumbling reorients them. The case of phoretic particles may be more complex[4,9], and may depend on the dynamics of the chemicals reacting at the swimmers surface. Schaar *et al.* recently showed that hydrodynamic torques strongly affect the "detention times" over which microswimmers reside near no-slip walls[10]. The behaviour is partly controlled by the details of the force distribution with which active particles stir the surrounding fluid; previous work has shown that these details also control the behaviour of spherical squirmers near a flat surface[11,12].

Previous theories have not systematically studied the effects of a short range repulsion between the particle and the wall; in experiments, such repulsive interactions are typical, either due to screened electrostatics, for charged walls, or due to steric interactions, *e.g.* for polymer-coated surfaces. Here we show that explicitly including this repulsion is important, and strongly affects the dynamics near a surface. The interplay between hydrodynamics and short range repulsion can lead to trapping, periodic oscillations, and to a swimming speed significantly different from that in the bulk. These results provide an experimentally viable route to tune microswimmer concentration and speed near a no-slip surface. Furthermore, recent theoretical calculations[11] predict that the equations of motion for squirmers which are pushers (exerting extensile forces on the fluid) do not possess any stationary bound state solution, *i.e.,* where the particle swims stably along the wall at fixed orientation. Our finding of oscillatory near-wall dynamics shows that even without such stationary solutions, trapping of swimmers at walls is possible. We show that this behaviour requires near-field hydrodynamic interactions and that the observed oscillatory dynamics can be explained by a theoretical model combining far and near-field contributions.

[a] *Laboratoire de Physique des Solides, CNRS, Univ. Paris-Sud, Université Paris-Saclay, 91405 Orsay Cedex, France.*
[b] *SUPA, School of Physics and Astronomy, University of Edinburgh, UK.*
[c] *EPCC, School of Physics and Astronomy, University of Edinburgh, UK.*

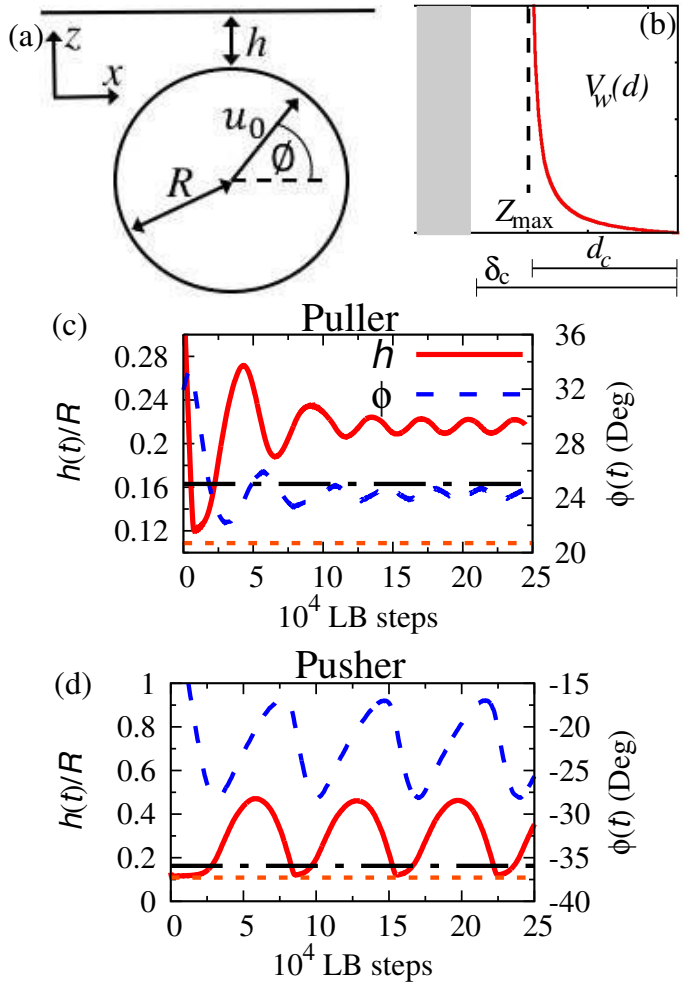

Fig. 1 (a) A cartoon showing an example of a squirmer near a flat wall, defining the gap size h and angle ϕ used in the text. In the bulk, the squirmer would move with speed u_0 along the direction shown, at an angle ϕ from the horizontal. (b) There is a repulsive interaction between the wall and the squirmer. Examples of steady state $\phi(t)$ (dashed (blue) line) and $h(t)$ (solid (red) line) observed for (c) puller ($\beta = +5$) and (d) pusher ($\beta = -5$) dynamics near a flat wall in the absence of thermal noise are also shown. The interaction range is $\delta_c \sim 0.16R$ (dot-dashed line) and the potential diverges at $\sim 0.11R$ (dotted line).

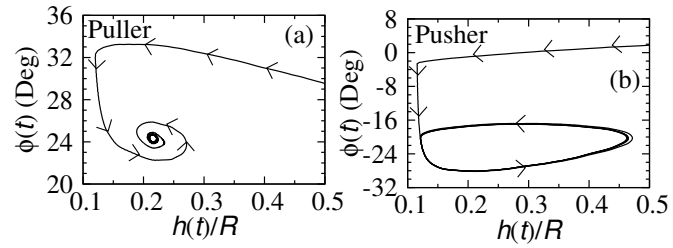

Fig. 2 Trajectories of the squirmers in (h, ϕ) space, showing a fixed point for (a) a $\beta = +5$ puller and a limit cycle for (b) a $\beta = -5$ pusher. The repulsive range was $\delta_c \approx 0.16R$ (initial conditions $h_0 \approx 3.25R$ and $\phi_0 = 10°$; no thermal noise).

2 Model and methods

2.1 Squirmer model

A popular model for swimmer hydrodynamics is a spherical squirmer – a particle which is rendered self-motile through a surface slip velocity[13]. The squirmer model has been used to study, e.g., the collective motion and nutrient uptake of swimmers in thin films[14,15]. To study the dynamics of a model squirmer in confinement we employ a lattice Boltzmann (LB) method[16]. To achieve time independent squirming motion, the following tangential (slip) velocity profile at the particle surface is used [17]

$$u(\theta) = 2\sum_{n=1}^{\infty} \frac{\sin\theta}{n(n+1)} \frac{dP_n(\cos\theta)}{d\cos\theta} B_n \qquad (1)$$

where θ is the polar angle and P_n is the nth Legendre polynomial[11].

In the LB method a no-slip boundary condition at the fluid/solid interface can be achieved by using the standard method of bounce-back on links (BBL)[18,19]. When the boundary is moving (*e.g.* a colloidal particle) the BBL condition must be modified to take into account particle motion[20]. These local rules can include additional terms, such as a surface slip velocity (Eq. 1): in this way it is possible to simulate squirming motion[21,22]. Our implementation also includes thermal noise[23], allowing for simulations with a finite Péclet number.

2.2 Simulation parameters

We limit our simulations to simple squirmers with $B_n = 0$, for $n \geq 3$, but consider both pushers ($B_2 < 0$) and pullers ($B_2 > 0$). In simulation units (SU) we measure the lengths in lattice spacings and time in simulation steps. Parameters, all given in SU are: $B_1 = 0.0015$, $B_2 = \pm 0.0075$, (which gives a swimming velocity in the bulk equal to $u_0 = \frac{2}{3}B_1 = 10^{-3}$ and $\beta \equiv \frac{B_2}{B_1} = \pm 5$), fluid viscosity $\eta = 0.1$. We carried out simulations with and without thermal noise. For simulations with thermal noise we used $k_BT = 10^{-5}$. We considered a fully resolved swimmer with radius $R = 9.2$ (Fig. 1(a)). The physics is governed by two main hydrodynamic dimensionless quantities: the Reynolds and Péclet numbers. Using the parameters above, these are $\mathrm{Re} = \frac{u_0 R}{\eta} \approx 0.09$ as well as both infinite Pe and $\mathrm{Pe} = \frac{u_0}{D_r R} \approx 2 \times 10^4$ respectively, where $D_r = \frac{k_BT}{8\pi\eta R^3}$, is the rotational diffusion constant. Our simulations were carried out in a cuboidal simulation box $120 \times 120 \times 96$, with periodic boundary conditions in X and Y and solid walls at $z = 0$ and $z = 95$. By matching the viscosity η to the kinematic viscosity of water $\eta \sim 10^{-6}\frac{\mathrm{m}^2}{\mathrm{s}}$, we can map a single length and time SU to $\sim 1\mu$m and 0.1μs, respectively. These would correspond to $R \sim 9$ μm, $u_0 \sim 10\frac{\mathrm{mm}}{\mathrm{s}}$, and a distance between walls of $\sim 100\mu$m. Note that while the mapped swimming speed is higher than observed in experiments, the requirement of $\mathrm{Re} << 1$ is fulfilled.

In order to model the wall-particle repulsion, we employ a soft potential

$$V_{\mathrm{W}}(d) = V(d) - V(d_c) - (d - d_c)\left.\frac{\partial V(d)}{\partial d}\right|_{d=d_c}, \qquad (2)$$

where the separation $d \equiv d(z) = Z_{max}^{min} \pm z - R$ is the distance be-

tween the particle surface and the position where the potential diverges ($Z_{\max}$ ($Z_{\min}$) for top (bottom) walls) and

$$V(d) = \varepsilon\,(\sigma/d)^{\nu}\,. \tag{3}$$

$V_{\rm W}(d)$ has been cut-and-shifted to ensure that the potential and force go smoothly to zero at $d = d_c$. Parameters were chosen as $\varepsilon = 0.004$, $\sigma = 0.1$, $\nu = 1.0$. By choosing $Z_{\max} = Z_{\rm top} - (\delta_c - d_c)$ ($Z_{\min} = Z_{\rm bottom} + (\delta_c - d_c)$) and keeping $d_c = 0.5$SU constant, we can have a well defined repulsion range δ_c, while keeping d_c and thus the potential form constant (Fig.1(b)). For the calculation of the gap size between the squirmer and the solid surface h (Fig. 1(a)), we define the wall location half-way between the solid node and the first fluid node ($Z_{\rm bottom} = 0.5$ and $Z_{\rm top} = 94.5$), as customary in LB simulations.

3 Results

3.1 Periodic swimming near a repulsive surface

In Fig. 1(c,d) we plot the evolution of the dimensionless gap size $\varepsilon = h(t)/R$ and of the angle ϕ between the squirmer direction and the surface plane (Fig. 1(a)). For a puller, after an initial collision with the soft repulsive wall, the hydrodynamically induced torques rotate the particle so that in steady state it swims parallel to the no-slip wall (beyond the excluded volume interaction range; dot-dashed line in Fig. 1(c)) with a distance $h \sim 0.2R$, in very good agreement with theoretical predictions[11]. In steady state the puller points towards the surface, $\phi \sim 24$ degrees (Fig. 1(c)). For a $\beta = -5$ pusher, previous theories based only on hydrodynamic interactions predict no stable swimming near a surface[11]. However, in experiments, phoretic swimmers which are thought to be pushers for mechanistic reasons[24], are typically observed to accumulate and undergo stable swimming at no-slip surfaces[2,4].

Strikingly, our simulations (Fig. 1(d)), show a stable periodic orbit both in $h(t)$ and $\phi(t)$. During a collision with the soft-repulsive wall, hydrodynamic torques reorient the pusher (Fig. 1(d)) leading to it swimming away from the wall (ϕ is on average < 0 in Fig. 1(d)). This much is expected; surprisingly, the hydrodynamic interactions between the swimmer and the wall then pull the pusher towards the wall even though it remains oriented away from it. The cycle repeats leading to hydrodynamic oscillations (Fig. 1(d)). This is even more apparent from the squirmer trajectories in (h,ϕ) space, which show a fixed point for a puller, in agreement with theoretical predictions[11] and the appearance of a limit cycle for a pusher as shown in Fig. 2. Experimentally, these observed oscillations could be difficult to distinguish from true, steady-state trapping, providing a potential explanation for the experimental observations. Cyclic swimming and decaying cyclic swimming in h have been previously reported for *pullers* in refs.[12] and[21]. Interestingly, a recent theoretical study has also reported transient oscillatory trajectories around the central plane between two parallel surfaces[25]. Those oscillations are well explained by far-field hydrodynamics. The oscillations are dependent on initial conditions, which is why we have not observed them here.

For both pushers and pullers, the hydrodynamically induced attraction is strong enough to resist, to some degree, the effects of thermal noise, i.e., a finite Péclet number, see Fig. 3. However, we were unable to approach experimentally realistic noise levels (which correspond to Pe ~ 50) in reasonable simulation times. (Reducing Pe would require proportionate reduction in swimming speed u_0, and thus proportionally longer simulation runs to obtain the same statistics). Another possibility would be to reduce the particle size. However we chose to maintain a reasonably large particle ($R = 9.2$) in order to have well resolved flow fields near the particle surface and thus achieve small surface separations. Ref.[20] reports that hydrodynamics is well-resolved in LB for passive spheres moving near walls down to separations of $0.1R$, which is below the minimum separation in our simulations.

Decreasing β reduces the strength of hydrodynamic torques[4]. $\beta = 0$ corresponds to a neutral squirmer with a quadrupolar flow field near the particle: fluid velocity $v \propto r^{-3}$, with r the distance from the swimmer centre. When $|\beta| > 0$ a stresslet contribution is included and the longest-range flow field becomes dipolar, $v \propto r^{-2}$. Our choice of $\beta = \pm 5$ corresponds to reasonably strong pullers/pushers. The observed bulk swimming speed and stresslet contribution, from a recent experimental study of Janus swimmers inside a colloidal crystal[4], can be used to estimate $|\beta| \sim 4-8$. We carried out additional simulations where we reduced $|\beta|$. We observed no trapping at the wall for a neutral squirmer or weak pullers/pushers with $\beta = -2,\ 0$ or 2 (see Fig. 6 in appendix A.1).

3.2 Effects of the external soft repulsion

The external soft repulsion, and in particular its range, plays a key role in determining the swimming dynamics. This can be seen from the $\phi(t)$ and $h(t)$ curves presented in Fig. 3(a-d), for different repulsive ranges ($\delta_c = 0.16R,\ 0.22R$ and $0.27R$): these simulations include the effect of thermal noise, with Pe $\approx 2\times 10^4$, and were all initialised near the top wall and pointing towards it, with $h_0 \approx 1.1R$ and $\phi_0 = 45^\circ$. For all ranges considered, both the pusher and the puller are found to swim near the surface (Fig. 3(a,d)). However, the hydrodynamic oscillations in the pusher dynamics (visible both in $h(t)$ and $\phi(t)$ Fig. 3(a,b)) are suppressed when the repulsive range is increased, and disappear altogether for $\delta_c = 0.27R$ (Fig. 3). In this case, for both pusher and puller the steady state $h < \delta_c$. The plot of the swimming orientation $\phi(t)$ (Fig. 3(b,e)) confirms the absence of oscillations: the pusher swims by keeping a stable orientation tilted away from the wall, with ϕ slightly decreasing when δ_c is increased (Fig. 3(c)); the puller instead is rotated by hydrodynamic torques to point towards the wall, so that $\phi \sim 90^\circ$ (this is always the case as soon as $\delta_c \geq 0.22R$ (Fig. 3(f))).

3.3 Comparison to theoretical predictions

Most existing theories of swimmer hydrodynamics rely on the far-field approximation which is based on the velocity field a swimmer generates at distances which are large with respect to its size. The far-field approximation can be adapted to include a no-slip wall[26]: as a result one obtains the following expressions for the

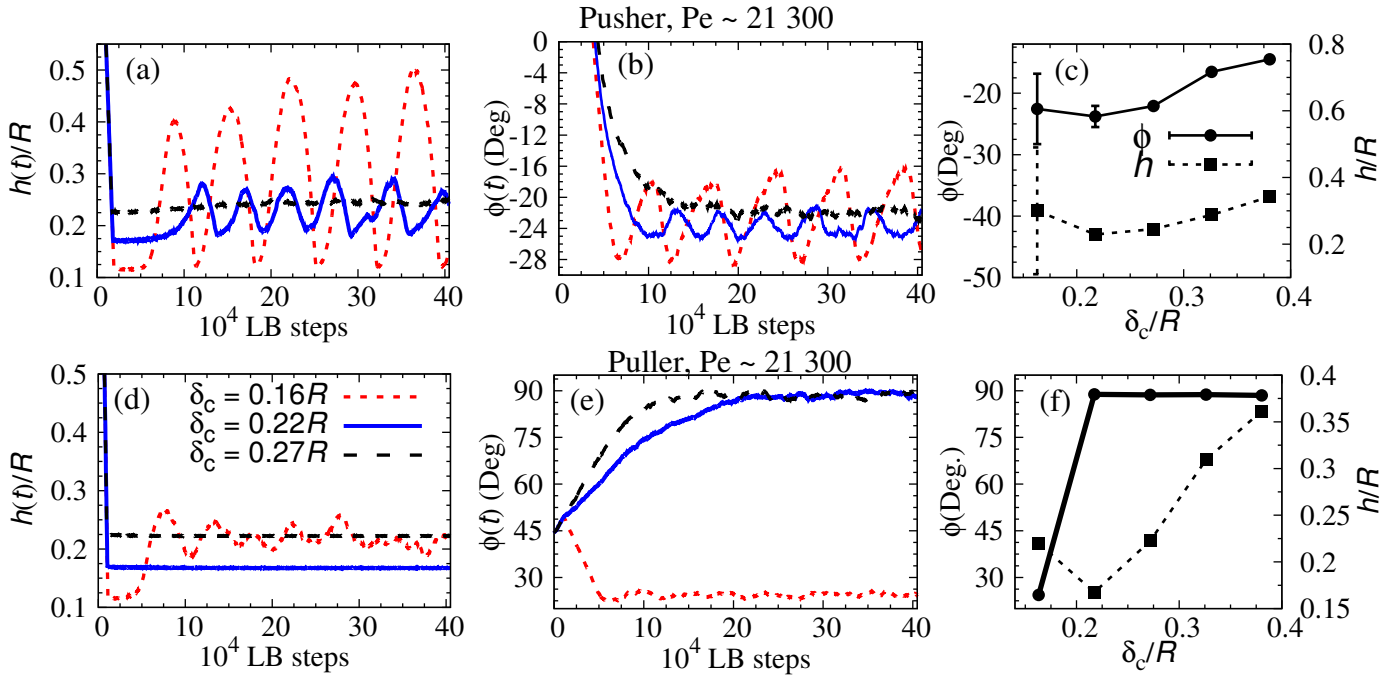

Fig. 3 Simulation results when the range of the soft repulsion is varied $\delta_c \approx 0.16R$ (dotted (red) line), $\delta_c \approx 0.22R$ (solid (blue) line) and $\delta_c \approx 0.27R$ (dashed (black) line), with $\mathrm{Pe} \approx 2 \times 10^4$ for a $\beta = -5$ pusher (top row) and a $\beta = +5$ puller (bottom row). Time development of $h(t)/R$ (a) for a pusher and (d) for a puller as well as $\phi(t)$ for (b) a pusher and (e) a puller. (The sudden change in behaviour for a puller is discussed in the text). The steady state h and ϕ as a function of δ_c for (c) a pusher (the errorbars gives the amplitude of the oscillations) and (f) a puller. (Initial conditions: $h_0 \approx 1.1R$ and $\phi_0 = 45.0°$; $\mathrm{Pe} \approx 2 \times 10^4$).

time derivative of ϕ at a given time,

$$\frac{\mathrm{d}\phi}{\mathrm{d}t} = \frac{u_0}{R}\left[\frac{9\beta\sin(2\phi)}{64}\left(\frac{R}{h'}\right)^3 - \frac{3\cos\phi}{16}\left(\frac{R}{h'}\right)^4\right] \quad (4)$$

where $\beta = \frac{B_2}{B_1}$ and h' is the distance from the centre of the particle to the confining wall ($h' = h + R$ in Fig. 1(a)), and we have truncated the expression at $\mathscr{O}[(R/h')^4]$ as in Ref.[26]. Eq. (4) was obtained by rewriting the results of Ref.[26] in terms of squirmer modes using Ref.[11]. We also use lubrication theory to compute the following prediction, based on near-field hydrodynamics[10,27,28],

$$\frac{\mathrm{d}\phi}{\mathrm{d}t} = -\frac{3u_0}{2R}(1+\beta\sin\phi)\cos\phi + \mathscr{O}\left(\frac{1}{\log\varepsilon^{-1}}\right) \quad (5)$$

which should apply when the dimensionless gap size $\varepsilon = (h' - R)/R$ is small (see appendix A.3 and A.4 for further details and for the derivation of the lubrication results). We were unable to obtain lubrication results for the translational swimmer velocity, which is why we focus on the rotational dynamics.

To allow comparison between our model and the theoretical predictions (Eq. 2 and 3), we carried out simulations starting with $h_0 \approx 3.25R$ and $\phi_0 = 10°$ and at each point in time, we calculated the expression for $d\phi/dt$ either directly from our numerics, or by substituting the instantaneous values of $h(t)$ and $\phi(t)$ into Eq. 4 and 5: these two equations respectively provide the far- and near-field estimate of the system evolution given its current state and can be combined by means of a matched asymptotic expansion (see appendix A.5 for further details).

For early times, there is good agreement between the rotational dynamics, $d\phi/dt$, predicted by the far-field approximation and that found in our direct numerical simulations (Fig. 4): we observe a decrease (pusher) and increase (puller) of $\phi(t)$ from the initial $\phi_0 = 10°$. Later on, the far-field estimate no longer captures the dynamics observed in simulation. In steady state, the far field predicts $\frac{d\phi}{dt} > 0$ while simulations show no net motion of $\phi(t)$, as shown in Fig. 3(b,e). By incorporating the near-field contribution, we obtain good agreement between the theory and our simulations, including the trapping of the puller and the oscillations of the pusher (Fig. 4). This is achieved by tuning two free parameters which have identical values for the pusher and the puller (see appendix A.5 for further details on matching the far and near-field contributions). This result can be understood by noting that the far- and near-field contributions are qualitatively different. In the far-field, a pusher swims stably parallel to the wall, whereas a puller rotates until it is perpendicular to it[26]. In the near-field, it is the puller which swims stably along the wall, pointing slightly towards it[11], whereas the pusher has no stable swimming solution. In our simulations, the particle is trapped close to the wall, so near-field hydrodynamics dominates, although far-field contributions are non-negligible (as detailed in appendix A.3). An analysis of the dynamics of approach to the surface, dz/dt, leads to similar conclusions: prior to interacting with the repulsive wall, the far-field works well; when the repulsive interaction is reached, there is a notable disagreement (see Fig. 7 in appendix A.1). However, we were unable to obtain a near-field prediction for dz/dt or dx/dt (see below) in order to

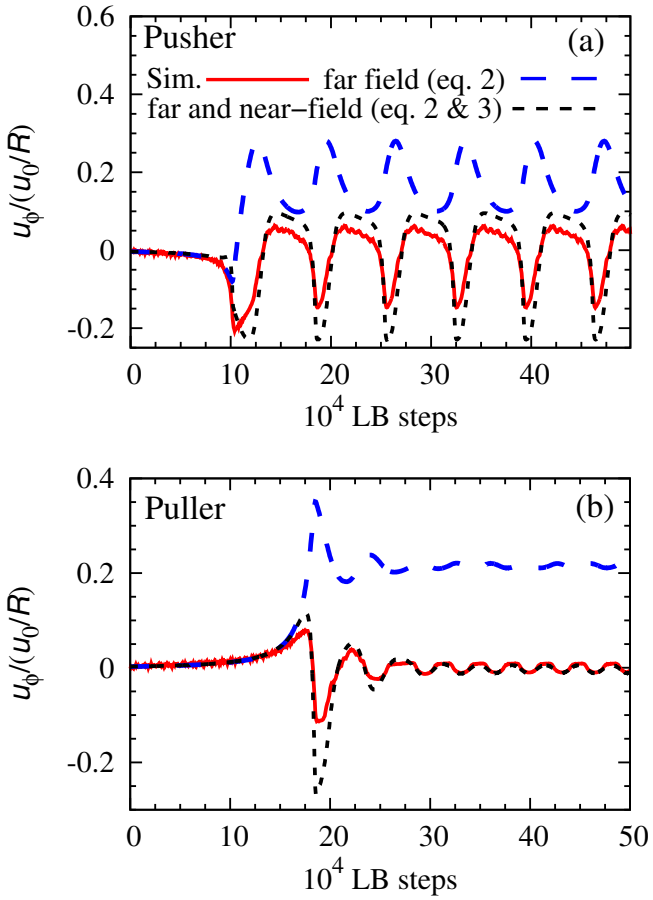

Fig. 4 Observed simulation (solid (red) line), far field (dashed (blue) line) and combined near and far-field (dotted (black) line), results for $u_\phi(t)/(u_0/R)$ for (a) pusher ($\beta = -5$) and (b) puller ($\beta = +5$). The repulsive range was $\delta_c \approx 0.16R$ (initial conditions $h_0 \approx 3.25R$ and $\phi_0 = 10°$; no thermal noise).

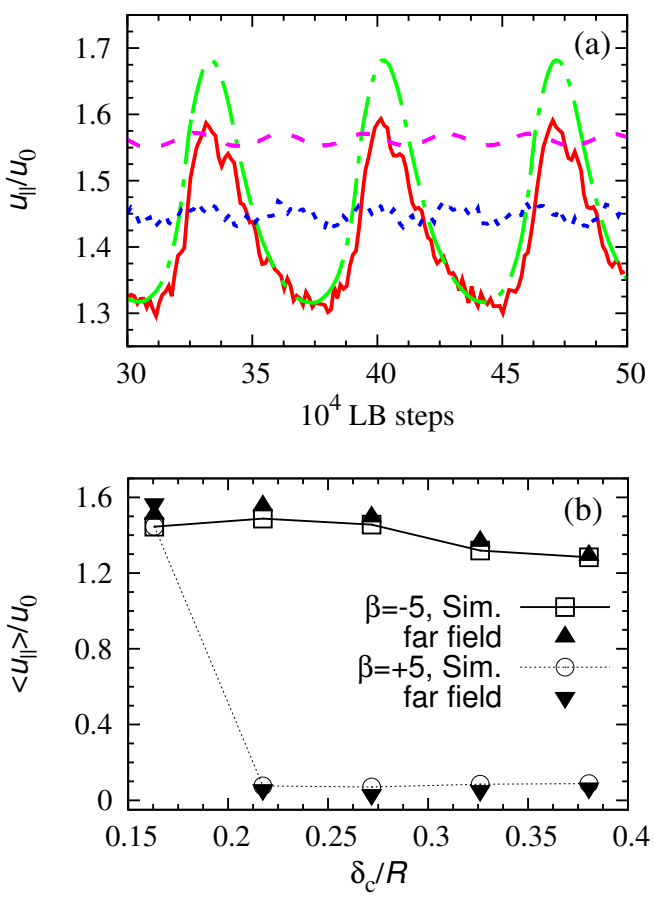

Fig. 5 (a) Simulations and far field results for the observed steady state swimming speed along the wall $u_\parallel(t)/u_0$ for a pusher ($\beta = -5$); simulations (solid (red) line) and far field predictions (dot-dashed (green) line) and puller ($\beta = +5$); simulations (dotted (blue) line) and far field prediction (dashed (pink) line). ($\delta_c \approx 0.16R$; initial conditions: $h_0 \approx 1.1R$, $\phi_0 = 45°$; no thermal noise). (b) Time averaged $\langle u_\parallel \rangle/u_0$ as a function of the repulsion range δ_c, from simulations (open symbols) and far field calculations (closed symbols), for both pushers (squares and upward triangles) and pullers (circles and downward triangles). Initial conditions: $h_0 \approx 1.1R$, $\phi_0 = 45°$; Pe $\approx 2 \times 10^4$.

match the simulation results because the lowest order term is zero in both cases (see Appendix A.3 and A.4 for further details).

3.4 Variable swimming speed along the wall

For movement along the wall ($dx/dt \equiv u_\parallel$), the simulations and far field predictions agree reasonably well at all times (Fig. 5(a); similar conclusions were reached by Spagnolie and Lauga[26]). The steady state velocities for both swimmers are considerably larger than in the bulk, i.e. the presence of a surface accelerates the motion ($\sim 50\%$ increase, see Fig. 5(a)). The increase in the swimming speed near a solid surface can be understood intuitively by considering the swimming mechanism. The pusher is propelled from behind, thus when pointing away from the surface it ejects flow backwards against a solid wall – this should enhance the swimming speed, as predicted for swimmers in porous media[4,29]. The speed increase is retained for the periodic swimming. This is because, in spite of the angular oscillations, the pusher always points away from the wall (see Fig. 3(b)). Now $u(t)$ oscillates, as could be expected, but retains, on average, $u(t) \sim 1.5u_0$ (solid line in Fig. 5(a)). The speedup of the puller can be understood in a similar way: the squirmer is now oriented towards the wall so by pulling fluid inward along its swimming axis, it pulls itself along the wall. There is limited data on the comparative behaviour of phoretic particles near surfaces, but recent experiments do report an enhanced swimming speed up to $\sim 2u_0$ for Janus colloids next to a water-air interface[30].

Increasing the range of the repulsive interaction leaves the pusher dynamics along the surface mostly unaffected: we find that $u_\parallel > u_0$ for all the interaction ranges considered, as shown in Fig. 5(a,b). The case of the puller is very different, as any repulsive interaction extending past the equilibrium swimming distance $\sim 0.2R$ leads to hydrodynamic torques orienting the particle towards the wall (Fig. 3(e,f)); see also appendix A.1 for Fig. 8, which shows that the far-field approximation for the tangential speed remains good in this case as well). The reorientation occurred with all the initial conditions we considered (in Fig. 4(b)

the initial angle is almost tangential, $\phi_0 = 10^\circ$), and leads to a dramatic slowing down of the particle, whose motion virtually comes to a standstill when $\delta_c \geq 0.22R$ (see Fig. 5(b)).

In all the cases we have considered, the rotational motion plays a fundamental role in the dynamics of the particle, and this is affected by δ_c. The soft repulsion only slows down the particle movement along the surface normal (as visible from Fig. 7 for dz/dt in appendix A.1), and it *does not* create any torques; therefore any rotational motion of the particle only arises from the combination of hydrodynamic and Brownian forces.

4 Discussion

We have presented a study of fully resolved spherical squirmers swimming between two solid walls, using a microscopic model which prescribes a slip velocity at the particle surface. Our results show that repulsive interactions, which have been neglected in previous theories of swimmers interacting with surfaces, play a very important role in the squirmer's dynamics. First, they can stabilise hydrodynamic oscillations of a pusher close to the wall. A recent systematic investigation has demonstrated that in the parameter range we consider ($-5 \leq \beta \leq 0$) there is no stable bound state with the pusher swimming near the wall.[11], but experiments routinely observe that bacteria (which are known to be pushers) and phoretic swimmers (which are thought to be pushers) are attracted to and swim near flat surfaces[2,6]. One way to reconcile these results is if the trajectory of the swimmer at long times is oscillatory (a limit cycle in the (h,ϕ) plane) instead of having constant velocity (a stationary point in the (h,ϕ) plane). While this conclusion should hold qualitatively for several different pusher swimmers, we note that a spherical squirmer model does not provide a quantitatively accurate description of a rod-like bacterial swimmer such as *E.coli*, so that the details of its hydrodynamic oscillations may in practice differ from those presented here. With respect to bacterial accumulation at surfaces, it should be noted that the repulsion range considered here, $\delta_c \geq 0.16R$, is larger than could be expected to arise, for example, from electrostatic interactions in a typical bacterial media. However, it remains relevant for experiments on artificial synthetic swimmers which typically employ much lower salt concentrations, and hence exhibit longer electrostatic screening lengths.

Second, we find that the swimming speed of a pusher is much increased with respect to the bulk limit: this behaviour can be understood as the swimmer, on average, is directed away from the wall and pushes on it, enhancing its speed. Third, we find that the tangential velocity of a puller slows down dramatically with the range of the repulsive interaction with the wall. Our results critically require near-field hydrodynamics, as the far-field approximation poorly captures the rotational dynamics we observe.

Our findings further imply that by tuning the extent of the repulsion, properties such as the number density and speed of active particles near a surface, could be controlled. Experimentally this could be achieved, by varying either the buffer concentration (for electrostatic repulsion) or the polymer coverage of the surface (for steric repulsion). These predictions should be testable with experiments using bacterial swimmers or artificial microswimmers, although for phoretic particles one may need to first estimate the effect of chemical gradients, here neglected, on the dynamics[4,9,31–33].

A Appendix

A.1 Additional figures

In this section we provide three additional figures (Fig. 6-8). Figure 6 shows the gap size $h(t)/R$ as a function of time, when the squirming parameter β is varied as $\beta = 0, \pm 2$. In figure 7 observed simulation results and far-field predictions for the swimming speed perpendicular to the wall u_z/u_0 are presented for a $\beta = -5$ pusher and a $\beta = +5$ puller, respectively. It shows a disagreement between the far-field prediction (eq. (7)) and observed simulations results, which persists also after correcting the far-field to include an extra normal velocity component arrising from the external repulsive potential, $u_w = -\frac{1}{\gamma}\frac{\partial V(d)}{\partial d}$, where $\gamma = 6\pi\eta R$. Finally in figure 8 the swimming speed along the wall u_x/u_0 is presented for both a pusher and a puller when the interaction range is $\delta_c \approx 0.22R$. In this case the observed simulation results for u_x agree well with the predictions from far-field theory given by equation (6).

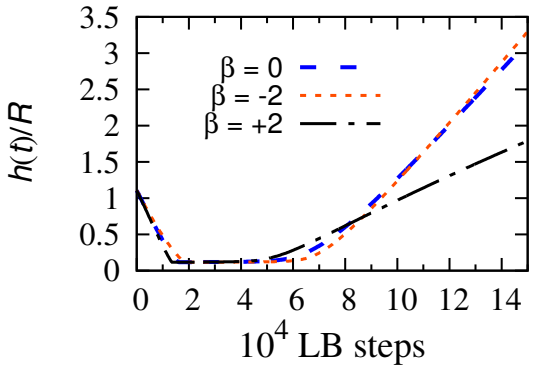

Fig. 6 Observed simulation results for $h(t)/R$ for a neutral squirmer ($\beta = 0$; dashed (blue) line), for a pusher ($\beta = -2$; dotted (red) line) and for a puller ($\beta = +2$; dot-dashed (black) line). The repulsive range was $\delta_c \approx 0.16R$ and $\mathrm{Pe} \approx 2 \times 10^4$.

A.2 Far-field approximation

The far-field approximation is based on the velocity field which a swimmer generates at distances which are large with respect to its size. The far-field approximation can be adapted to include a no-slip wall[26]: as a result one obtains the following expressions for the time derivative of the positions parallel x and perpendicular z as,

$$\frac{\mathrm{d}x}{\mathrm{d}t} = u_0\left[\cos\phi + \frac{9\beta\sin(2\phi)}{32}\left(\frac{R}{h'}\right)^2 - \frac{\cos\phi}{8}\left(\frac{R}{h'}\right)^3\right] \quad (6)$$

$$\frac{dz}{dt} = u_0\left[\sin\phi - \frac{9\beta\left(1-3\sin^2\phi\right)}{32}\left(\frac{R}{h'}\right)^2 - \frac{\sin\phi}{2}\left(\frac{R}{h'}\right)^3\right] \quad (7)$$

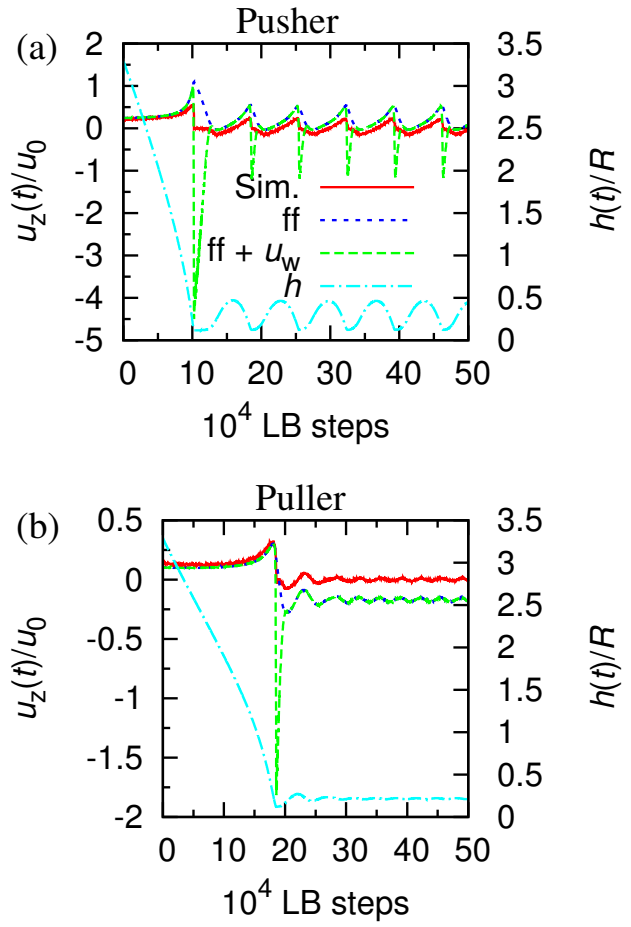

Fig. 7 Observed simulation results (solid (red) line and dot-dashed (light blue) line) and far field results (dotted (blue) line) for $u_z(t)/u_0$ for (a) pusher and (b) puller. The disagreement between simulations and far-field approximation persists after correcting the latter to include the repulsive interaction from the wall, via an extra normal velocity equal to $u_w = -\frac{1}{\gamma}\frac{\partial V(d)}{\partial d}$ (where $\gamma = 6\pi\eta R$) (dashed (green) line). The appearance of the sharp peaks, when u_w is included, result from the interaction with the repulsive potential. The repulsive range was $\delta_c \approx 0.16R$ (initial conditions $h_0 \approx 3.25R$ and $\phi_0 = 10°$; no thermal noise).

where $\beta = \frac{B_2}{B_1}$ and h' is the distance from the centre of the particle to the confining wall ($h' = h + R$ in Fig. 1(a) in the main text), and we have truncated the expression at $\mathcal{O}[(R/h')^3]$ as in Ref.[26].

A.3 Lubrication Results

In Ref.[34], the wall-parallel force F_x and torque T_y on a squirmer moving near a no-slip boundary is calculated. We repeat these calculations in Section A.4. We obtain different prefactors for F_x and T_y compared to Ref.[34], but we agree as to the functional form. In summary, our corrected results for a squirmer oriented at angle ϕ away from the parallel to the plane (see Fig. 9) are

$$F_x = -\frac{4\pi\eta R u_c}{5}\log(1/\varepsilon) + \mathcal{O}(1), \tag{8}$$

$$T_y = \frac{16\pi\eta R^2 u_c}{5}\log(1/\varepsilon) + \mathcal{O}(1). \tag{9}$$

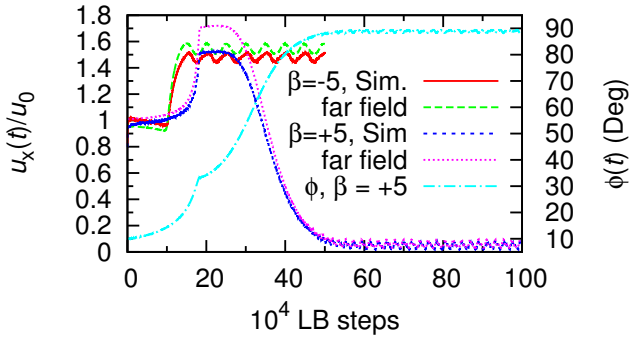

Fig. 8 Simulations and far field results for the velocity along the wall $u_x(t)/u_0$ for pusher ($\beta = -5$) (simulations solid (red) line and far field dashed (green) line) and puller ($\beta = +5$) (simulations short-dashed (blue) line and far field dotted (pink) line) as well as $\phi(t)$ for a puller ($\beta = +5$) (dot-dashed (light blue) line), when the repulsion range was $\delta_c \approx 0.22R$ (initial conditions $h_0 \approx 3.25R$, $\phi_0 = 10°$; no thermal noise).

Here, u_c is the surface slip velocity (parallel to the wall) at the point of closest approach ($\times$) between the squirmer and the wall, which, for the squirmer defined in Eq. 1 of the main text is

$$u_c = -u(\pi/2 - \phi) = -\frac{3}{2}u_0\cos\phi\,(1 + \beta\sin\phi)\,. \tag{10}$$

From standard results for the drag on a sphere near a wall[35] the force and torque give simple expressions for the *total* rotation Ω and speed u_x of the squirmer

$$\Omega = \frac{\mathrm{d}\phi}{\mathrm{d}t} = \frac{u_c}{R} + \mathcal{O}(1/\log\varepsilon)\,, \tag{11}$$

$$u_x = \frac{\mathrm{d}x}{\mathrm{d}t} = 0 + \mathcal{O}(1/\log\varepsilon)\,. \tag{12}$$

or, in terms of u_0 and ϕ

$$\begin{aligned}\frac{\mathrm{d}\phi}{\mathrm{d}t} &= -\frac{3}{2}\frac{u_0}{R}\cos\phi\,(1 + \beta\sin\phi) + \mathcal{O}\left(\frac{1}{\log\varepsilon}\right)\\ \frac{\mathrm{d}x}{\mathrm{d}t} &= 0 + \mathcal{O}\left(\frac{1}{\log\varepsilon}\right).\end{aligned} \tag{13}$$

In other words, the term of order unity in the total translational motion of a squirmer near a wall vanishes, and the leading order speed decays as $\mathcal{O}(1/\log\varepsilon)$ as the squirmer approaches the wall. It is not possible to calculate the numerical value of this term from lubrication theory, since it depends on longer-range interactions between the whole squirmer and the wall[35]. Since this logarithmic decay is very weak, the leading order term will remain comparable to u_0 except for squirmers extremely close to surfaces. In the current simulations $\varepsilon \gtrsim 0.1$, giving $|1/\log\varepsilon| \gtrsim 0.4$, which is not small. Hence, it is not contradictory that, in simulations, we see u_x increase as the squirmer approaches the wall: this is probably because the swimmer does not approach the wall very closely in the simulations. The lubrication calculations merely predict that, for a sufficiently close approach, the translational speed of the squirmer will begin to decrease and eventually slow to zero. For

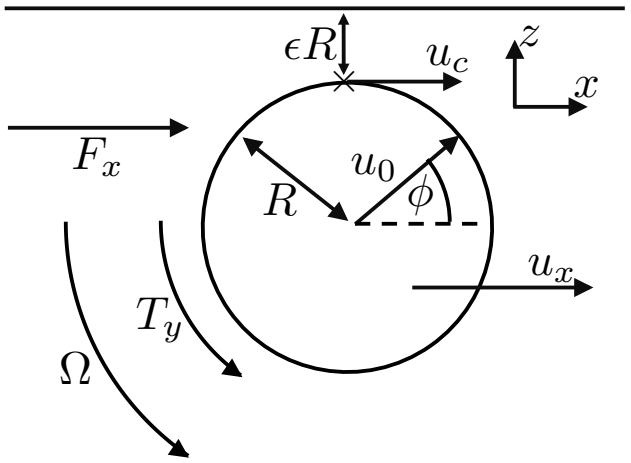

Fig. 9 Definition of the geometry of a spherical squirmer of radius R next to a plane surface. The $\hat{\mathbf{y}}$ direction is into the page. In the bulk, the squirmer would move at speed u_0 along the direction shown, at angle ϕ from the horizontal. The squirmer is axisymmetric around this axis. u_c is the slip velocity at the point of closest approach, indicated by $\times$. At this point, the squirmer wall gap is εR. The fluid flow generates a force F_x and torque T_y on the squirmer, around its centre, which generate translation at speed u_x along the x-axis, and rotation, at angular velocity Ω around the y-axis.

the vertical speed, u_z, the term of order unity also vanishes[34], so we do not calculate u_z here. For the rotational motion, the next-to-leading order term also decays as $\mathcal{O}(1/\log\varepsilon)$, so it will also be significant.

We can provide an intuitive justification for Eq. (11)-(12). As the swimmer gets closer and closer to the surface, most of the viscous dissipation will occur in the thin region around the contact point. We would therefore expect the solution to minimise the dissipation in this region. This can be done by ensuring that there is no difference in fluid velocity between the particle and the plane surface at this point of contact. Hence, the total velocity on the particle surface, taking into account the slip velocity and the solid-body motion of the particle should, in the limit of infinitesimal gap size, approach zero, i.e.,

$$\lim_{\varepsilon\to 0}\left(u_c + u_x - R\Omega\right) = 0\,. \tag{14}$$

This condition is satisfied (but not uniquely) by Eq. (11)-(12). It is not satisfied by the original result derived in Ref.[34].

A.4 Calculation of Lubrication Force and Torque

We briefly repeat here the lubrication calculations of Ref.[34], to obtain the results in Eq. (8)-(9). This calculation is identical to the standard calculation of the forces and torques of a no-slip sphere near a surface[35], except for the new boundary condition on the sphere surface introduced by the finite slip velocity.

We will calculate F_x and T_y, which are the force and torque produced on the squirmer by its squirming motion when it is held fixed relative to the wall, translationally and rotationally. To do this, we define a cylindrical coordinate system (ρ^*, z, ψ), with $\rho^{*2} = x^2 + y^2$ and $\tan\psi = y/x$, where the origin of the coordinate system is the point on the plane immediately above the squirmer's centre. The boundary of the squirmer is defined by $z = h(\rho^*, \phi)$, and in the vicinity of the contact point is given by

$$h = -R\left(\varepsilon + \frac{\rho^{*2}}{2R^2} + \mathcal{O}\left(\frac{\rho^{*4}}{R^2}\right)\right). \tag{15}$$

To ensure that the equations of motion are all of order unity, we use the dimensionless stretched variables X, Y, Z, H, ρ, with the scaling

$$\varepsilon^{1/2}RX = x,\ \ \varepsilon^{1/2}RY = y,\ \ \varepsilon^{1/2}R\rho = \rho^* \tag{16}$$

$$\varepsilon RZ = z, \quad \varepsilon RH = h\,. \tag{17}$$

The stretched height H is

$$H = -1 - \frac{\rho^2}{2} + \mathcal{O}(\varepsilon)\,. \tag{18}$$

The fluid velocity field $\mathbf{u}$ has x, y, z components u, v and w respectively. In the stretched coordinate system, the Stokes equations are

$$\eta\left(\varepsilon\nabla_\parallel^2 + \frac{\partial^2}{\partial Z^2}\right)\mathbf{u} = R\varepsilon\left(\varepsilon^{1/2}\frac{\partial p}{\partial X},\quad \varepsilon^{1/2}\frac{\partial p}{\partial Y},\quad \frac{\partial p}{\partial Z}\right), \tag{19}$$

$$\varepsilon^{1/2}\left(\frac{\partial u}{\partial X} + \frac{\partial v}{\partial Y}\right) + \frac{\partial w}{\partial Z} = 0\,. \tag{20}$$

where $\nabla_\parallel = \hat{\mathbf{x}}\partial/\partial X + \hat{\mathbf{y}}\partial/\partial Y$ and with fluid viscosity η and pressure p. No-slip boundary conditions apply on the plane surface: $\{u, v, w\}|_{Z=0} = 0$, and we write the boundary velocity on the upper surface as $u(Z=H) = U$, $v(Z=H) = V$ and $w(Z=H) = W$. Expanding the boundary conditions as power series in orders of $\varepsilon^{1/2}$ around $\rho = 0$, we have

$$U = u_c + \mathcal{O}(\varepsilon^{1/2})\,, \tag{21}$$

$$V = 0 + \mathcal{O}(\varepsilon^{1/2})\,, \tag{22}$$

$$W = 0 - u_c\varepsilon^{1/2}\rho\cos\psi + \mathcal{O}(\varepsilon)\,. \tag{23}$$

Performing a similar expansion for the velocity and pressure in the thin swimmer-surface gap gives

$$u = u_0 + \varepsilon^{1/2}u_1 + \mathcal{O}(\varepsilon)\,, \tag{24}$$

$$v = v_0 + \varepsilon^{1/2}v_1 + \mathcal{O}(\varepsilon)\,, \tag{25}$$

$$w = 0 + \varepsilon^{1/2}w_0 + \varepsilon w_1 + \mathcal{O}(\varepsilon^{3/2})\,, \tag{26}$$

$$p = \varepsilon^{-3/2}\left[p_0 + \varepsilon^{1/2}p_1 + \mathcal{O}(\varepsilon)\right]. \tag{27}$$

Here, the subscripts 0 and 1 indicate the leading and next-to-leading order components of the solution. Here, we will derive only the leading order terms. From Eq. (19), p_0 is independent of Z. Integrating Eq. (19) over Z and solving for u_0 and v_0 then

gives

$$u_0 = \frac{R}{2\eta}\frac{\partial p_0}{\partial X}(Z-H)Z + \frac{Z}{H}u_c\,, \tag{28}$$

$$v_0 = \frac{R}{2\eta}\frac{\partial p_0}{\partial Y}(Z-H)Z\,. \tag{29}$$

Combining these solutions and using the equation of continuity (Eq. (20)) yields, after some algebra

$$\frac{H^3R}{12\eta}\nabla_\parallel^2 p_0 - \frac{H^2R}{4\eta}\rho\cdot\nabla_\parallel p_0 - \frac{1}{2}u_c\rho\cos\psi = 0\,. \tag{30}$$

Inserting the ansatz $p_0 = q_0(\rho)\cos\psi$ then gives an equation in terms of ρ alone

$$\frac{H^3R}{12\rho^2\eta}\frac{\partial}{\partial\rho}\left(\rho\frac{\partial q_0}{\partial\rho}\right) - \frac{H^3R}{12\rho^3\eta}q_0 - \frac{H^2R}{4\eta}\frac{\partial q_0}{\partial\rho} + \frac{1}{2}u_c = 0\,. \tag{31}$$

which has the particular solution

$$q_0 = -\frac{6\eta\rho}{5H^2R}u_c\,. \tag{32}$$

As discussed in[34], the conditions that p_0 be finite everywhere means that this is the only physically relevant solution.

Next, we rewrite the x,y velocities in the cylindrical polar coordinate system, i.e.,

$$\mathbf{u} = u_\rho\hat{\rho} + u_\psi\hat{\psi} + u_z\hat{\mathbf{z}}\,. \tag{33}$$

Using the ansatz

$$u_\rho = \cos\psi\tilde{u}_\rho(\rho)\,, \tag{34}$$

$$u_\psi = \sin\psi\tilde{u}_\psi(\rho)\,, \tag{35}$$

we obtain for the in-plane components

$$\tilde{u}_\rho = \frac{R}{2\eta}(Z-H)Zq_0' + \frac{Z}{H}u_c\,, \tag{36}$$

$$\tilde{u}_\psi = -\frac{R}{2\eta}(Z-H)Z\frac{q_0}{\rho} - \frac{Z}{H}u_c\,, \tag{37}$$

where the prime indicates the radial derivative $\partial/\partial\rho$.

To obtain the total horizontal force F_x on the swimmer, we integrate small elements of force over the swimmer surface S, i.e.,

$$F_x = \int_S \mathrm{d}F_x\,, \tag{38}$$

where[35]

$$\mathrm{d}F_x = \hat{\mathbf{x}}\cdot\sigma\cdot\hat{\mathbf{n}}\mathrm{d}S\,, \tag{39}$$

with σ the stress tensor, and $\mathrm{d}S$ an infinitesimal area element. We evaluate the stress tensor in cylindrical polar coordinates, but use spherical polar coordinates centred on the particle centre, with the polar angle $\chi = 0$ at the point of closest approach, to specify the normal $\hat{\mathbf{n}}$. This gives

$$\mathrm{d}F_x = \left[-p\sin\chi\cos\psi + \eta\left(\sin\chi\cos\psi\tau_{\rho*\rho*} - \sin\chi\sin\psi\tau_{\pi\rho*} + \cos\chi\cos\psi\tau_{\rho*z} - \cos\chi\sin\psi\tau_{\psi z}\right)\right]\mathrm{d}S\,. \tag{40}$$

where τ is the rate of strain tensor, with components (in the unstretched coordinates z,ψ,ρ^*)

$$\tau_{\rho*\rho*} = 2\frac{\partial v_\rho}{\partial\rho*}\,, \qquad \tau_{\psi\rho*} = \rho*\frac{\partial}{\partial\rho*}\left(\frac{v_\psi}{\rho*}\right) + \frac{1}{\rho*}\frac{\partial v_\rho}{\partial\psi}\,,$$

$$\tau_{\rho*z} = \frac{\partial v_\rho}{\partial z} + \frac{\partial v_z}{\partial\rho*}\,, \qquad \tau_{\psi z} = \frac{\partial v_\psi}{\partial z} + \frac{1}{\rho*}\frac{\partial v_z}{\partial\psi}\,, \tag{41}$$

and $\mathrm{d}S = R^2\sin\chi\mathrm{d}\chi\mathrm{d}\psi$ is the area increment in spherical polar coordinates. Inserting the expansions for the velocities and rescaling into the stretched coordinates gives

$$\mathrm{d}F_x = \left\{-\varepsilon^{-3/2}q_0\sin\chi\cos^2\psi + \frac{\eta}{R}\left[2\varepsilon^{-1/2}\sin\chi\cos^2\psi\frac{\partial\tilde{u}_\rho}{\partial\rho} - \varepsilon^{-1/2}\sin\chi\sin^2\psi\left(\rho\frac{\partial}{\partial\rho}\left(\frac{\tilde{u}_\psi}{\rho}\right) - \frac{1}{\rho}\frac{\partial\tilde{u}_\rho}{\partial\psi}\right) + \right.\right. \tag{42}$$

$$\left.\left. + \cos\chi\cos^2\psi\left(\varepsilon^{-1}\frac{\partial\tilde{u}_\rho}{\partial Z} + \frac{\partial\tilde{u}_z}{\partial\rho}\right) - \cos\chi\sin^2\psi\left(\varepsilon^{-1}\frac{\partial\tilde{u}_\psi}{\partial Z} - \frac{1}{\rho}\frac{\partial\tilde{u}_z}{\partial\psi}\right)\right]\right\}\mathrm{d}S\Big|_{Z=H}\,. \tag{43}$$

Performing the integral over ψ gives

$$F_x = R^2\pi\int_0^\pi\left\{-\varepsilon^{-3/2}q_0\sin\chi + \frac{\eta}{R}\left[2\varepsilon^{-1/2}\sin\chi\frac{\partial\tilde{u}_\rho}{\partial\rho} - \varepsilon^{-1/2}\sin\chi\left(\rho\frac{\partial}{\partial\rho}\left(\frac{\tilde{u}_\psi}{\rho}\right) - \frac{1}{\rho}\frac{\partial\tilde{u}_\rho}{\partial\psi}\right) + \right.\right.$$

$$\left.\left. + \cos\chi\left(\varepsilon^{-1}\frac{\partial\tilde{u}_\rho}{\partial Z} + \frac{\partial\tilde{u}_z}{\partial\rho}\right) - \cos\chi\left(\varepsilon^{-1}\frac{\partial\tilde{u}_\psi}{\partial Z} - \frac{1}{\rho}\frac{\partial\tilde{u}_z}{\partial\psi}\right)\right]\right\}\sin\chi\mathrm{d}\chi\Big|_{Z=H}\,. \tag{44}$$

To perform the integral over χ, we expand to first order around $\chi = 0$, giving $\sin\chi = \varepsilon^{1/2}\rho + \mathscr{O}(\varepsilon)$. The inner, lubrication region extends to some real distance ρ_0^* of order the particle size, $\rho_0^* = DR$, where $D = \mathscr{O}(1)$ is an unknown constant which can be obtained by matching to the outer solution. In the stretched coordinate system, the corresponding limit is $\rho_0 = D\varepsilon^{-1/2}$. To lowest order

$$F_x = R^2\pi\int_0^{\rho_0} -q_0\rho^2 + \frac{\eta\rho}{R}\left(\left.\frac{\partial\tilde{u}_\rho}{\partial Z}\right|_{Z=H} - \left.\frac{\partial\tilde{u}_\psi}{\partial Z}\right|_{Z=H}\right)\mathrm{d}\rho\,, \quad (45)$$

and evaluating this integral gives

$$F_x = -\frac{8\pi\eta R u_c}{5}\log(\rho_0) + \mathscr{O}(1)\,. \quad (46)$$

We wish to express F_x in terms of ε. As discussed in Ref.[34,35], we do not need to determine the unknown constant D in order to do this, because $\log\rho_0 = -(1/2)\log\varepsilon + \log D$, so the value of D can be absorbed into the $\mathscr{O}(1)$ term. Hence we obtain the expression in Eq. (8).

The torque T_y can be calculated in the same way by integrating the differential elements of torque[34]

$$\mathrm{d}T_y = R\left[(\hat{\mathbf{n}}\cdot\hat{\mathbf{z}})\hat{\mathbf{x}} - (\hat{\mathbf{n}}\cdot\hat{\mathbf{x}})\hat{\mathbf{z}}\right]\cdot\sigma\cdot\hat{\mathbf{n}}\mathrm{d}S\,, \quad (47)$$

giving, after the same steps as above, the integral

$$T_y = R^3\pi\int_0^{\rho_0}\frac{\eta\rho}{R}\left(\left.\frac{\partial\tilde{u}_\rho}{\partial Z}\right|_{Z=H} - \left.\frac{\partial\tilde{u}_\psi}{\partial Z}\right|_{Z=H}\right)\mathrm{d}\rho\,, \quad (48)$$

which yields the expression in Eq. (9). As stated in the previous section, standard results then give the speed and rotational velocity of the squirmer when it is not held fixed. From Ref.[35], to lowest order

$$\Omega = \frac{RF_x + 4T_y}{12\pi\eta R^3\log(1/\varepsilon)}\,, \quad (49)$$

$$u_x = \frac{4RF_x + T_y}{12\pi\eta R^2\log(1/\varepsilon)}\,, \quad (50)$$

which gives Eq. (11)-(12).

A.5 Matching Lubrication and Far-field Results

In order to obtain a result which can be compared with the simulation results everywhere, we perform a matched asymptotic expansion of the near-field and far-field results. We define $q = R/h' = 1/(1+\varepsilon)$. Then, the far-field corresponds to $q \to 0$, while the near-field corresponds to $\varepsilon \to 0$. In the near-field, the next-to-leading-order term is $\mathscr{O}(1/\log\varepsilon)$, so, in order to match this term to the far-field we define the function

$$f(q) = \frac{2q}{\log\left(\frac{1+q}{1-q}\right)}\,, \quad (51)$$

which has the near-field limit $f \to -2/\log(\varepsilon)$, and the far-field limit $f \to 1$. For intermediate values, $f(q)$ is smooth and monotonic. We then use the following matched expansion

$$\frac{1}{Ru_0}\frac{\mathrm{d}\phi}{\mathrm{d}t} = \cos\phi q^4\left[-\frac{3}{2} + \left(\frac{21}{16} + c_1q^2\right)f(q)\right] + \beta\sin(2\phi)q^3\left[-\frac{3}{4} + \left(\frac{57}{64} + c_2q^2\right)f(q)\right]\,, \quad (52)$$

where c_1 and c_2 are constants to be determined by matching to the simulations. This expansion matches both the lubrication results and the far-field results in their respective domains of applicability, with corrections of $\mathscr{O}(1/\log\varepsilon)$ in the near field, and $\mathscr{O}(\beta q^5)$ and $\mathscr{O}(q^6)$ in the far-field, which is the next order of approximation there[26]. There are two next-to-leading-order terms in the far-field because we have linearly independent contributions from the $n = 1$ and $n = 2$ Legendre components of the slip velocity.

With the fitting parameters, $c_1 = 1$, $c_2 = 0.29$, we obtain semi-quantitative agreement with the simulation results. Because of the very slow decay of the next-to-leading-order terms in the lubrication theory, we would not expect an exact match. Thorough testing of the lubrication theory would require simulations where the swimmer approaches much closer to the plane surface.

Acknowledgements

We thank Andreas Zöttl and Joost de Graaf for fruitful discussions. This work was funded by EU intra-European fellowship 623637 DyCoCoS FP7-PEOPLE-2013-IEF and UK EPSRC grant EP/J007404/1

References

1 Lord Rothschild, *Nature*, 1963, **198**, 1221.
2 A. T. Brown and W. C. K. Poon, *Soft Matter*, 2014, **10**, 4016–4027.
3 D. Takagi, J. Palacci, A. B. Braunschweig, M. J. Shelley and J. Zhang, *Soft Matter*, 2014, **10**, 1784.
4 A. T. Brown, I. D. Vladesdu, A. Dawson, T. Visser, J. Schwarz-Linek, J. S. Lintuvuori and W. C. K. Poon, *Soft Matter*, 2016, **12**, 131–140.
5 P. Galadja, J. Keymer, P. Chaikin and R. Austin, *J. Bacteriol.*, 2007, **189**, 8704.
6 A. P. Berke, L. Turner, H. C. Berg and E. Lauga, *Phys Rev Lett*, 2008, **101**, 038102.
7 G. Li and J. X. Tang, *Phys Rev Lett*, 2009, **103**, 78101.
8 J. Elgeti and G. Gompper, *EPL*, 2013, **101**, 48003.
9 W. E. Uspal, M. N. Popescu, S. Dietrich and M. Tasinkevych, *Soft Matter*, 2015, **11**, 434–438.
10 K. Schaar, A. Zöttl and H. Stark, *Phys. Rev. Lett.*, 2015, **115**,

038101.
11 K. Ishimoto and E. A. Gaffney, *Physical Review E*, 2013, **88**, 062702.
12 G.-J. Li and A. M. Ardekani, *Phys. Rev. E*, 2014, **90**, 013010.
13 M. J. Lighthill, *Communications on Pure and Applied Mathematics*, 1952, **5**, 109–118.
14 A. Zöttl and H. Stark, *Phys. Rev. Lett.*, 2014, **112**, 118101.
15 R. A. Lambert, F. Picano, L. Brandt and W. P. Breugem, *J. FLuid. Mech.*, 2013, **733**, 528.
16 M. E. Cates, K. Stratford, R. Adhikari, P. Stansell, J.-C. Desplat, I. Pagonabarraga and A. J. Wagner, *J. Phys. Condens. Mater.*, 2004, **16**, S3903.
17 V. Magar, T. Goto and T. J. Pedley, *Quart. J. Mech. Appl. Math.*, 2003, **56**, 65.
18 A. J. C. Ladd, *J. Fluid Mech.*, 1994, **271**, 285.
19 A. J. C. Ladd, *J. Fluid Mech.*, 1994, **271**, 311.
20 N.-Q. Nguyen and A. J. C. Ladd, *Phys. Rev. E*, 2002, **66**, 046708.
21 I. Llopis and I. Pagonabarraga, *J. Non-Newtonian Fluid Mech.*, 2010, **165**, 946.
22 I. Pagonabarraga and I. Llopis, *Soft Matter*, 2013, **9**, 7174.
23 R. Adhikari, K. Stratford, M. E. Cates and A. J. Wagner, *Europhys. Lett.*, 2005, **71**, 473.
24 S. Das, A. Garg, A. I. Campbell, J. Howse, A. Sen, D. Velegol, R. Golestanian and S. J. Ebbens, *Nat. Commun.*, 2015, **6**, 8999.
25 J. de Graaf, A. J. T. M. Mathijssen, F. M., M. H., H. C. and S. T. N., *Soft Matter*, 2016, **12**, 4704.
26 S. E. Spagnolie and E. Lauga, *J.Fluid Mech.*, 2012, **700**, 105.
27 A. Zöttl, *Ph.D. thesis*, Technischen Universität Berlin, 2014.
28 B. Cichocki and R. Jones, *Phys. Rev. Lett.*, 1998, **258**, 273.
29 R. Ledesma-Aguilar and J. M. Yeomans, *Phys. Rev. Lett.*, 2013, **111**, 138101.
30 X. Wang, M. In, C. Blanc, M. Nobili and A. Stocco, *Soft Matter*, 2015, **12**, 7376–7384.
31 I. Theurkauff, C. Cottin-Bizonne, J. Palacci, C. Ybert and L. Bocquet, *Phys. Rev. Lett.*, 2012, **108**, 268303.
32 T. Bickel, A. Majee and A. Würger, *Physical Review E*, 2013, **88**, 012301.
33 F. Ginot, I. Theurkauff, D. Levis, C. Ybert, L. Bocquet, L. Berthier and C. Cottin-Bizonne, *Phys. Rev. X*, 2015, **5**, 011004.
34 T. Ishikawa, M. P. Simmonds and T. J. Pedley, *J. Fluid Mech.*, 2006, **568**, 119–160.
35 S. Kim and S. J. Karrila, *Microhydrodynamics: principles and selected applications*, Courier Dover Publications, 2013.